CrossMark

JFM PAPERS

A head-driven model of turbine fence performance

D. Dehtyriov[1],†, C.R. Vogel[1] and R.H.J. Willden[1]

[1]Department of Engineering Science, University of Oxford, Oxford OX1 3PJ, UK

This paper presents an analytic model for the analysis of co-planar turbine fences that partially span the width of a channel in which the flow is driven by a sinusoidally oscillating driving head. The thrust presented by the turbines reduces the flow rate through the channel leading to a solution for overall power that is dependent upon turbine resistance and flow blockage as well as on channel characteristics. We introduce a return parameter, in terms of power per turbine area, to assess optimum turbine fence deployment for a given channel. We find that the optimal deployment rests on a universal curve independent of the channel characteristics, and that these characteristics – namely the integrated channel bed friction and a modified channel Froude number – move the optimum along this curve. We find that blockage considerations play a large role in the performance of a tidal farm – its achievable power, optimal return, channel flow rate reduction and device thrust – and that the scales of blockage must be considered even when designing relatively unblocked farms. The impact of the channel characteristics on the optimal arrangement, alongside environmental constraints that may limit permissible flow blockage, are quantified and discussed.

Key words: channel flow, coastal engineering, shallow water flows

1. Introduction

Many advances have been made on the theoretical modelling of tidal turbine performance in confined channels. The work of Garrett & Cummins (2007) demonstrated the importance of considering the impact of blockage (flow confinement) on the upper limit of energy extraction for a homogeneously arrayed turbine fence that completely spans the width of the channel under the assumption of an undeforming free surface. This upper limit increases from the Betz limit typically assumed for unconstrained wind turbines in

† Email address for correspondence: daniel.dehtyriov@eng.ox.ac.uk

proportion to the square of the relative confinement. Corrections have been applied to tidal turbines to account for the deformation of the free surface (Whelan, Graham & Peiró 2009). Nishino & Willden (2012) extended the model by considering a long turbine fence that only partially spans the width of a channel, allowing for incomplete channel use that may be necessitated in practical turbine arrangements, for example due to bathymetric variations or shipping lanes. Here, two scales of flow confinement are considered: a local blockage (ratio of turbine frontal area to local flow passage area) dependent on tip-to-tip spacing between adjacent turbines, and a global blockage effect due to the channel geometry constraints. This model, working on the basis of scale separation between turbine and array scale flow events, located a new energy extraction limit for a closely packed tidal turbine fence in an infinitely wide channel of 79.8 % of the kinetic energy flux of the undisturbed approach stream, achieved at a local blockage ∼0.4. Additionally, the model has been applied to multiple rows of tidal turbines (Draper & Nishino 2014), where it was found that a single row of turbines outperforms a staggered arrangement, and to shallow channels with non-negligible bed friction, which was found to change both the power extraction potential and the optimum fence arrangement (Creed *et al.* 2017). The scale-separation effect has been demonstrated experimentally using porous discs (Cooke *et al.* 2015), and power uplift through the local blockage effect has been shown in large laboratory turbine experiments (McNaughton *et al.* 2022).

These flow confinement models, however, assume a fixed flow rate through the channel. Garrett & Cummins (2005) developed a channel dynamics model that accounted for the sinusoidally varying channel head as well as the response of the channel flow rate to the resistance presented by the turbines. The tidal turbine farm is modelled as a single modifiable drag (or bed-friction) coefficient in a one-dimensional channel, for which it is found that the maximum power results from a balance between increasing the drag coefficient to increase power production and the associated reduction in channel flow rate that reduces power production. A later extension by Vennell (2010) allowed for the response of the channel flow rate to the resistance presented by the turbines spanning the entire channel width by taking into account blockage effects predicted by Garrett & Cummins (2007). Additionally, the models have been applied to other problems such as multiple channels (Cummins 2013) and bays connected to oceans (Blanchfield *et al.* 2008).

One of the key purposes of these models is to help to determine the tidal stream resource of a tidal channel site. The models provide a well-defined upper bound on the resource, and have been used widely to assess tidal power potential (Sutherland, Foreman & Garrett 2007; Karsten *et al.* 2008; O'Hara & Gallego 2017). However, the models either assume that the turbines occupy the full channel width or rely on numerical approximations. Vennell (2013) additionally analysed the efficiency of a tidal farm based on an actual site, and found that exceeding the Betz limit needs additional careful consideration of structural load and blockage constraints. Refinements to the upper bound have been considered, with Adcock *et al.* (2013) locating a new upper-bound estimate for an actual site by numerically considering wake mixing losses, enabling the calculation of the power usefully available for extraction as opposed to the total power removed from the flow.

Whilst these models have significantly improved on the Betz limit for estimating tidal power efficiency, they still fall short of representing realistic turbine physics. In particular, although the Nishino & Willden (2012) model does consider finite length fences, and is therefore appropriate for the realistically achievable low global blockages, it is restricted to a constant flow rate through the channel such that the turbine resistance has no influence on the channel dynamics. To address this issue, Gupta & Young (2017) proposed a quasi-steady theoretical model that combines the short fence extension to the two-scale
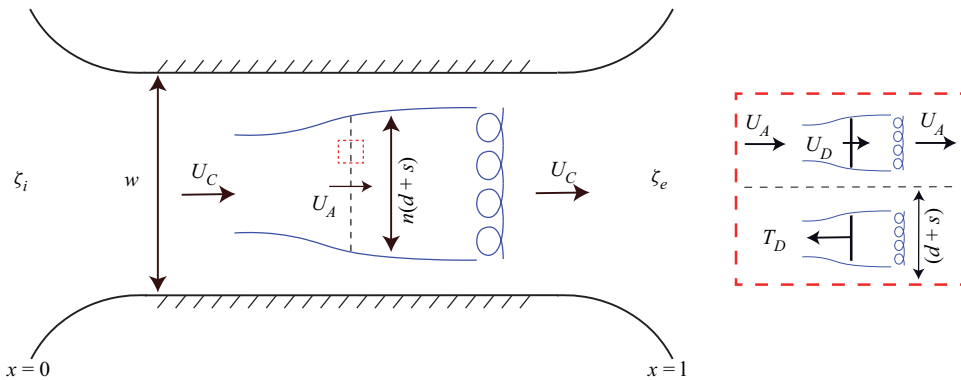
Figure 1. Schematic of a head-driven channel between two large basins in which a tidal turbine fence occupying part of the width of the channel is arrayed normal to the flow direction. An additional close-up view of a section of the fence shows the turbine scale flow problem. Remixing between core and bypass flows is shown for both turbine and fence scales.

theory (Nishino & Willden 2013) with both a free-surface deformation correction and the coupling of added drag with the upstream flow rate. Their flow rate model is based on a simplified static channel model detailed in Bryden & Couch (2007). A numerical framework was developed in the work of Bonar *et al.* (2019), where the two-scale model was embedded and coupled to realistic rough and oscillatory channel flows, for which the potential power capture was found to be greater as compared to the stand-alone steady-state two-scale model.

This paper presents a simplified analytic model that embeds the multi-scale partial fence model of Nishino & Willden (2012) in the channel dynamics model of Garrett & Cummins (2005), drawing on the work of Willden, Nishino & Schluntz (2014). The model allows for the analytic consideration of both rough bottom channels and oscillatory flow in a time-dependent framework, extending the work of Gupta & Young (2017). The model also accounts for the increase in performance due to local and global blockage effects, extending the works of Garrett & Cummins (2005) and Vennell (2010) to a fence partially spanning the channel width. As the work of Draper & Nishino (2014) has shown, for a fixed number of turbines, a single co-planar side-by-side row of turbines outperforms multi-row array arrangements, be they streamwise aligned or staggered; the model presented in this paper is restricted to a single fence of turbines partially spanning the width of a head-driven channel.

2. Finite-fence channel dynamics model

The flow problem is outlined by the sketch in figure 1, in which the flow is driven through the channel by a sinusoidally varying head difference between the channel ends. A turbine fence is positioned such that it partially occupies the width of the channel. The turbine fence consists of a large number n of closely spaced turbines, each of diameter d, that are arrayed with a tip-to-tip separation s in a plane normal to the channel flow direction.

The channel is simplified to be of rectangular cross-section with length l, width w and height h. The flow is driven by the elevation difference across the channel ends, $\zeta_i(t) - \zeta_e(t)$, which is assumed to vary sinusoidally in time with amplitude a and frequency ω. This forcing could be extended to account for higher-order interactions, for example the difference of sinusoidal tides at the ends of the channel. The resulting flow velocity through

the channel is then $U_C(t) = Q(t)/(wh)$, where $Q(t)$ is the flow rate, and both U_C and Q are functions of time alone due to the geometric simplification of constant channel cross-section, and an assumption that the driving tidal wave is far longer than the channel length (as per Garrett & Cummins 2005).

The flow through the turbine fence is modelled following the partial fence model of Nishino & Willden (2012) in which two scales of flow are considered: device scale flow and array scale flow. At the array scale, the resistance of the turbine fence causes flow diversion, resulting in an approach velocity U_A to the array that is lower than the stream velocity U_C. Similarly, at device scale, the resistance of each individual turbine causes flow to divert around each device such that the flow velocity through each device, U_D, is less than the array approach velocity U_A. Device scale mixing of device core and bypass flows occurs at dimensions scaling on the device diameter. This completes ahead of array scale mixing of array core and bypass flows, which occurs on dimensions scaling on the fence length. Through kinematic and dynamic coupling of the device, and array scales of the finite fence problem, the Nishino & Willden (2012) partial fence model provides a solution to the steady flow through the fence, and thus the power generated by the turbine fence, which may be parametrised conveniently by either turbine fence thrust or induction factor.

The Nishino & Willden (2012) partial fence model is a steady flow model and hence assumes implicitly that the upstream mass flux is unaffected by the resistance within the channel, which can be strictly true only at vanishingly small global blockage. By coupling the channel dynamics problem with an assumed quasi-steady partial fence model, the impact of fence resistance on channel flow rate can be incorporated so that the more relevant problem of the performance of a partial fence placed within a head-driven finite global blockage channel can be considered.

2.1. *Channel dynamics model*

The one-dimensional channel dynamics model of Garrett & Cummins (2005), which can be derived from the one-dimensional Euler equation, may be recast in non-dimensional form (the non-dimensional formulation was first presented in Willden *et al.* (2014) – see Appendix A for a complete derivation) as

$$\frac{\mathrm{d}Q'}{\mathrm{d}t'} - \cos t' = -\frac{1}{2} Q' |Q'| \frac{1}{Fr_\omega^2} \left(B_A C_{TA} + C_f \frac{l}{h} \right), \qquad (2.1)$$

in which the flow is driven through the (here presumed) rectangular cross-section channel by a sinusoidally varying head difference between the ends of the channel. Here, $Q' = Q/Q_0$ is the non-dimensional flow rate, in which $Q_0 = (ga/\omega)(wh/l)$ is the peak volume flow rate in the undisturbed channel (assuming negligible inflow and exit kinetic energy fluxes, and the absence of bed friction). Time t is non-dimensionalised according to $t' = \omega t$. This non-dimensionalisation has been applied previously by Muchala & Willden (2017) to investigate the impact of support structure drag on tidal turbine performance. In this model, however, the addition of the $B_A C_{TA}$ group indicates the extension to the internal coupling of the Nishino & Willden (2012) model.

The channel entry and exit are assumed smooth so that kinetic fluxes in and out of the channel may be neglected. The model equation (2.1) is an energy balance equation in which all terms are energy losses except for the driving head term $\cos t'$, which supplies energy to the channel. The unsteady term represents the energy required to accelerate the

flow through the channel, whilst the right-hand side represents the energy lost to overcome opposing (resistive) forces.

The resistance to the flow has two contributions: from bed friction, included through the friction coefficient C_f, and due to turbine array thrust, included through the array thrust coefficient

$$C_{TA} = \frac{T_A}{\frac{1}{2}\rho U_C^2 w_A h}, \tag{2.2}$$

in which T_A is the array thrust, $w_A = n(d + s)$ is the width of the turbine fence (array) and ρ is the fluid density. The proportion of the channel width occupied by the turbine fence is described by the array blockage ratio

$$B_A = \frac{w_A}{w}. \tag{2.3}$$

The flow characteristics in the empty channel are governed by the non-dimensional groups Fr_ω and l/h, and the bed friction C_f. Here, $Fr_\omega = \omega l/\sqrt{ga}$ takes the form of a Froude number and can be shown to be proportional to the square root of the ratio of cycle-averaged head supplied to the kinetic energy in the unresisted channel (see Appendix A). This channel-based Froude number describes the flow rate through the channel: for a fixed-geometry channel, increasing the amplitude of the tidal wave a (and thus decreasing Fr_ω) leads to an increase in flow rate through the channel, as expected. The product $C_f(l/h)$ provides the overall bed resistance, so increasing the depth of flow (and thus decreasing l/h) diminishes the importance of bed friction leading to an increase in the channel flow rate.

Specifying the product $C_f(l/h)/Fr_\omega^2$ enables solution of the channel flow problem in the absence of turbines. In the case of a turbine fence installation, we define the channel characteristics through specification of $C_f(l/h)$ and Fr_ω separately. The problem is then closed fully by specification of the proportion of the channel width occupied by turbines, B_A, and the array thrust coefficient C_{TA}, which is provided by kinematic and dynamic coupling to the partial fence model as outlined below. Although the resistive terms in the model equation (2.1) could be presented through two terms and hence two non-dimensional groups, as in Garrett & Cummins (2005), we choose here to use three, namely $C_f(l/h)$, Fr_ω and $B_A C_{TA}$, so as to separate properly channel characteristics from turbine characteristics.

Solution of the model equation (2.1) is achieved by time marching. Following several transient cycles, periodic solutions, of period $2\pi/\omega$, are obtained over which the time average farm thrust and power may be determined. The periodicity of the solution allows for alternative approaches to solving the model equation, particularly in the frequency domain. These could be considered for cases where rapid solutions are required, or where the phase spectrum is of direct interest. We also note that additional physical mechanisms may potentially increase the time-averaged power above the model predictions, such as dynamic effects following the change in tide direction (Bonar *et al.* 2019).

2.2. *Partial fence model*

Specification of the turbine fence thrust as a function of channel flow rate is sufficient to close the problem. Here, we use the partial fence model of Nishino & Willden (2012). The turbine fence is taken to lie in a plane normal to the flow direction, and the fence does not fully occupy the width of the channel as required from practical bathymetric and shipping

considerations; see figure 1. Hence the array approach flow is divided into an array core stream of velocity U_A, and an array bypass stream. The array core stream may itself be divided into n stream tubes, with each approaching a single device. Each device stream tube may again be divided into a device core stream, with flow speed through the device $U_D = U_A(1 - a_L)$, and a device bypass stream. Downstream of the array, we assume a separation of scales between device and array scale mixing. Device scale mixing, between the device core and bypass flows, scales on the device diameter d and occurs ahead of the start of array scale mixing, between the array core and bypass flows, which scales on the length of the array w_A. The model assumes implicitly that the fence is sufficiently long (large enough n) for this separation to be valid, and that the channel is sufficiently long – multiples of w_A – for array scale mixing to be completed within the channel. The numerical simulations of Nishino & Willden (2013) suggest that the restriction on n to achieve scale separation is not particularly onerous, with $n \geq 8$ achieving good agreement between theory and computation.

Each of the inner (device scale) problem and the outer (array scale) problem may be solved by application of the Garrett & Cummins (2007) model of device performance in a blocked flow passage. Their model extends the conservation of linear momentum theory, applied conventionally to unbounded wind turbines in which the outer flow can expand freely, to the case of a device in a finite cross-section flow passage in which the flow can no longer expand in an unconstrained manner. Such a geometric constraint results in the acceleration of the device bypass flow. It is assumed that downstream of the device, the core flow expands and the bypass flow contracts until a point of pressure equilibrium between the two streams is reached, following which the core and bypass flows remix to recover a uniform stream. Unlike the unbounded wind turbine theory, this blocked theory results in a solution in which a favourable pressure gradient is developed between the far upstream and downstream conditions. As in the Garrett & Cummins (2007) blocked device model, we here neglect changes in the free surface elevation and assume that the flow is bounded by a rigid lid. At the channel scale, however, following Garrett & Cummins (2005), we assume a channel depth that varies in time according to the driving tidal wave. Relaxation of the rigid-lid assumption at the device and array scales has a significant impact on only the model predictions for large Froude number ($Fr = U_C/\sqrt{gh}$) channels (Vogel, Houlsby & Willden 2016) or high global blockage ratios. As Froude numbers for realistic tidal channels are comparatively low ($0.1 \leq Fr \leq 0.2$; Vogel *et al.* 2016), and the results presented herein show peak performance points at modest global blockage ratios (see § 3), the rigid-lid assumption made in the partial fence model will introduce only small errors for practical turbine array deployment scenarios.

Starting with the inner device scale problem, we use the device scale thrust coefficient C_{TL} to non-dimensionalise the device scale thrust T_D through

$$C_{TL} = \frac{T_D}{\frac{1}{2}\rho U_A^2 \pi d^2/4}. \tag{2.4}$$

Applying the Garrett & Cummins (2007) model to the device scale problem enables this thrust coefficient to be evaluated through

$$C_{TL} = (1 - \gamma_L)\left[\frac{(1 + \gamma_L) - 2B_L(1 - a_L)}{(1 - B_L(1 - a_L)/\gamma_L)^2}\right], \tag{2.5}$$

in which γ_L is the ratio of the device scale wake velocity (at the device scale pressure equilibrium location) to the device approach velocity U_A, and B_L is the local blockage

956 A14-6

ratio defined as

$$B_L = \frac{\pi d^2/4}{(d+s)h},$$ (2.6)

in which the denominator is the cross-sectional area of the device scale flow passage. The ratio of device wake to approach velocity, γ_L, is related through mass conservation to the device induction factor a_L through

$$1 - a_L = \frac{1 + \gamma_L}{(1 + B_L) + \sqrt{(1 - B_L)^2 + B_L(1 - 1/\gamma_L)^2}}.$$ (2.7)

Once the local blockage has been specified, (2.5) and (2.7) may be solved for C_{TL} as a function of a_L alone. For each $0 < \gamma_L < 1$, (2.7) provides a unique solution $0 < a_L < 1$, which then solves for a unique C_{TL} in (2.5).

Following Nishino & Willden (2012), who first developed this two-scale model, we now apply the Garrett & Cummins (2007) model to the array scale problem, resulting in a similar form of equations that relate the array thrust coefficient C_{TA} to the array induction factor a_A, which itself relates the array approach flow velocity to the channel flow velocity through $U_A = U_C(1 - a_A)$. Once the array blockage B_A has been specified, the array thrust C_{TA} is parametrised by a_A as

$$C_{TA} = (1 - \gamma_A)\left[\frac{(1 + \gamma_A) - 2B_A(1 - a_A)}{(1 - B_A(1 - a_A)/\gamma_A)^2}\right],$$ (2.8)

in which γ_A is the ratio of array wake velocity (at the array scale pressure recovery location) to the upstream channel velocity U_C, related to the array induction a_A by

$$1 - a_A = \frac{1 + \gamma_A}{(1 + B_A) + \sqrt{(1 - B_A)^2 + B_A(1 - 1/\gamma_A)^2}}.$$ (2.9)

The device and array problems are coupled kinematically through the array approach velocity U_A, and dynamically through specifying the array thrust to be n times the device thrust, i.e. $T_A = nT_D$, or non-dimensionally,

$$C_{TA} = (1 - a_A)^2 B_L C_{TL}.$$ (2.10)

The kinematic and dynamic coupling closes the partial fence problem leading to a solution for array thrust as a function of device induction factor. Each device is assumed to be a perfect energy extractor so that it delivers power $P_D = T_D U_D$. Once device thrust, and device and array velocities, have been determined, the device local power coefficient C_{PL} and array global power coefficient C_{PG} may be determined trivially from

$$C_{PL} = \frac{P_D}{\frac{1}{2}\rho U_A^3 \pi d^2/4},$$ (2.11)

$$C_{PG} = \frac{nP_D}{\frac{1}{2}\rho U_C^3 n\pi d^2/4} = (1 - a_A)^3 C_{PL}.$$ (2.12)
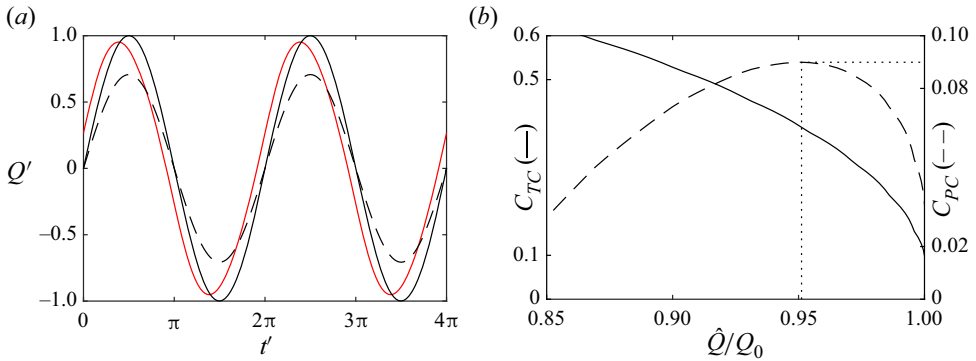
Figure 2. Example solutions to the channel flow rate over two tidal cycles. (*a*) The solid black line shows the undisturbed flow rate, the dashed line shows the flow rate assuming peak power production with homogeneous resistance in the Garrett & Cummins (2005) model and the solid red line shows the coupled fence–channel model flow rate for a specified fence geometry. (*b*) For a specified arrangement of turbines, the relationship between the peak flow rate reduction and the channel thrust and power coefficients. The peak power point locates the optimal thrust and necessary flow reduction for the specified arrangement.

2.3. *Coupled channel partial fence dynamics model*

For any given turbine layout, specified through the combination of local blockage B_L, which represents the spacing between turbines, and global blockage $B_G = B_L B_A$ (the ratio of total disc to channel cross-sectional areas), which represents the total number of turbines, the dynamic channel flow problem can be solved as a function of the applied fence thrust $B_A C_{TA}$. The partial fence model provides this non-dimensional group in (2.1) as a function of the array induction factor.

To couple the partial fence model to the channel flow model, we make the assumption that the fence operates at a constant array (or indeed device) induction factor across the entire tidal cycle; that is, we assume that the turbines in the fence operate solely with local knowledge so as to reduce the speed of the approach flow through the turbines by a fixed proportion (the induction factor) – as do wind turbines operating below rated flow speeds. The partial fence model may be solved conveniently in advance of the channel flow problem to provide the fence performance parametrised across the range of array induction factors $0 \leq a_A \leq 1$.

The Fr_ω and $C_f(l/h)$ groups are set based on the driving tidal wave, and channel geometry and bed friction estimates. Equation (2.1) is then integrated forwards in time until the peak amplitude of the channel flow rate, $\hat{Q}/Q_0$, converges across consecutive cycles. Figure 2 shows an example output Q/Q_0 for the peak performance point over two tidal cycles. Across the parameter space, the solution always converges to a periodic waveform, but not necessarily to a single-frequency cosine.

The solution presents in terms of a fence performance, which we assess through the cycle-averaged channel-based power coefficient C_{PC} across the range of array induction factors a_A, with each induction factor corresponding to an applied global thrust coefficient C_{TG} defined by

$$C_{TG} = \frac{C_{TA}}{B_L}, \tag{2.13}$$

which acts to reduce the amplitude of the flow rate by a factor $\hat{Q}/Q_0$. The thrust and power coefficients normalised by the peak channel flow rate (consistent with

Garrett & Cummins 2005) are defined by

$$C_{TC} = \frac{n\,T_{D,max}}{\rho g a A_C},\tag{2.14}$$

$$C_{PC} = \frac{n\,\overline{P_D}}{\rho g a Q_0},\tag{2.15}$$

where the overbar denotes a time average over a complete period of the driving tidal wave, and $T_{D,max}$ is the peak thrust over a tidal period.

As the channel thrust is increased, the flow rate through the channel is reduced (figure 2*b*). There is a consequent variation in the channel power, which at first increases until a peak performance is reached, before reducing as the channel flow rate is reduced too aggressively. This paper focuses on these optimal extraction points, which are unique for each set of turbine arrangements (B_L, B_G). Finally, we here define C_{TD} to be the peak single disc thrust

$$C_{TD} = \frac{T_{D,max}}{\rho g a A_T} = \frac{C_{TC}}{B_G},\tag{2.16}$$

as a metric to assess peak turbine loads. We assume that the channel and turbine peak resistances C_{TC} and C_{TD} are constant from cycle to cycle.

The partial fence formulation is the precursor step that provides one of the inputs to the channel dynamics model, and the two models may be conveniently solved sequentially. In discussion of model results, for each B_G and B_L, we concentrate on the fence thrust that results in the maximum C_{PC} as being the solution of interest to the channel–fence problem. To then map the performance over a range of B_L and B_G, this process may be repeated for $B_G \leq B_L \leq 1$, $0 \leq B_G \leq B_L$. In the absence of additional bed friction, the assumptions underpinning the limiting case as $B_L, B_G \to 1$ converge to the Garrett & Cummins (2005) channel model. In all cases where $C_f = 0$, the homogeneous array $(B_L, B_G \to 1)$ flow rate reduction therefore approaches near $\hat{Q}/Q_0 = 2^{-1/2}$, and peak power approaches $C_{PC} = 0.24$ (see, for example, figures 3(*a*) and 3(*c*), and the Garrett & Cummins (2005) homogeneous fence solution).

3. Finite fence performance in a head-driven channel

To contextualise the model results, we first consider typical tidal channel dimensions presented in table 1 (taken from Vennell & Adcock 2014), from which realistic ranges of the non-dimensional groups can be determined readily. As a reference case, we first consider a channel with a Fr_ω value between that of the two example channels listed in table 1. We then vary Fr_ω and consider the impact of bed friction assuming a typical bed-friction coefficient $C_f = 0.002$ across channel l/h ratios spanning the typical geometric ranges observed.

3.1. *Zero bed friction reference case*

An example solution for the head-driven array model is shown in figure 3 to demonstrate the impact of blockage on the fence performance in a channel with coupled upstream flow. This reference case is within the range of practical interest; we take lunar frequency $\omega = 1.4 \times 10^{-4}$ rad s^{-1}, equivalent to the dominant lunar M_2 frequency, and assume tidal amplitude $a = 0.5$ m, tidal turbine diameter $d = 20$ m, and channel length $l = 10$ km,
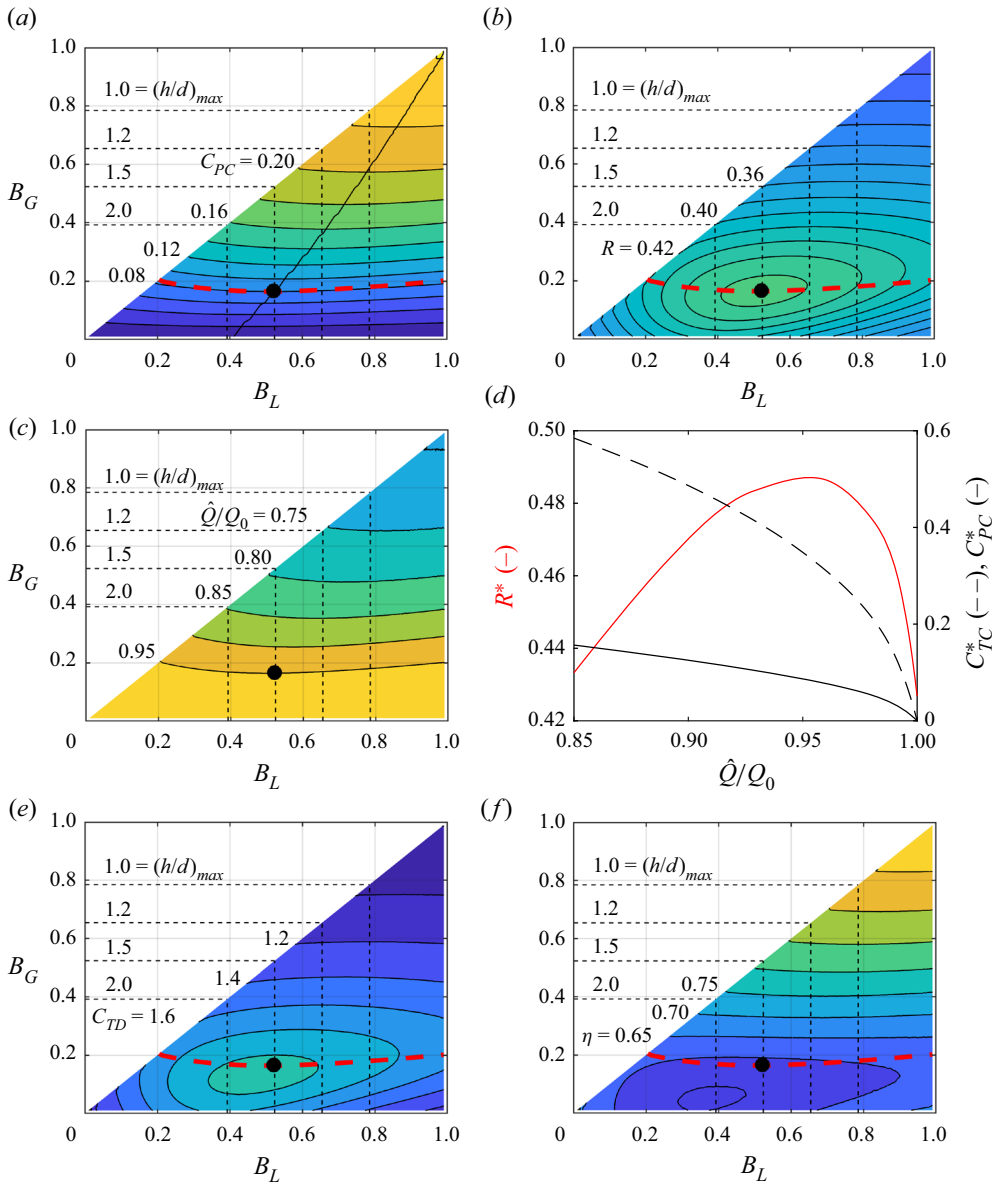
956 A14-9

Figure 3. Contours of fence performance for $Fr_\omega = 0.635$, $C_f = 0$, l/h undefined. All presented solutions correspond to the array thrust setting that achieves maximum C_{PC} at the indicated combination of blockage ratios. The black circle represents the maximum return point, and the red dashed line indicates the locus of $\hat{Q}/Q_0 = 0.95$. The dashed lines provide geometric limits on blockages for ratios of channel height h to turbine diameter d. (*a*) The channel power coefficient, with the solid black line indicating the locus of maximum C_{PC} with global blockage; (*b*) the return parameter; (*c*) the normalised peak flow rate; (*d*) the peak return, peak power coefficient and corresponding channel thrust across contours of normalised peak flow rate; (*e*) the disc thrust coefficient; (*f*) the basin efficiency.

resulting in a channel Froude number $Fr_\omega = 0.635$. For now, we assume that the channel bed friction C_f is negligible, but compare against cases with non-zero bed friction in § 3.3.

956 A14-10

	Length l (m)	Driving head amplitude a (m)	Depth h (m)	l/h	Fr_ω
Small tidal channel	5000	0.26	20	250	0.438
Pentland Firth	20 000	0.9	50	400	0.946

Table 1. Example channel dimensions based on a hypothetical small channel and the Pentland Firth.

The channel power coefficient C_{PC}, contoured in figure 3(*a*), increases with increasing global blockage. For any given global blockage (or specified flow reduction factor $\hat{Q}/Q_0$), there exists a corresponding B_L to maximise power generation, much as in the steady flow partial fence model (Nishino & Willden 2012). The physics of this increase in extractable power by local and global blockage mechanisms is discussed in detail in Dehtyriov *et al.* (2021). We additionally define the return parameter

$$R = \frac{C_{PC}}{B_G} \propto \frac{\text{total power extracted}}{\text{total frontal turbine area}}, \tag{3.1}$$

which may be interpreted usefully as income (power generated) per cost (turbine area). The maximum return, and the corresponding optimal turbine layout (B_L and B_G), can be determined from the model. Figure 3(*b*) shows the contours of the return parameter for the reference flow case, with the optimum indicated. For large channels where the turbine fence is expected to occupy a small proportion of the channel cross-section ($B_G \to 0$), there remains an optimal spacing B_L to maximise return. Increasing B_G then increases the peak return at a new optimal B_L, with the largest return ratio in this case realised for $B_G \approx 0.18$, $B_L \approx 0.49$. Further increases in B_G then allow higher levels of achievable channel power C_{PC} at the cost of a lower return, i.e. there are diminishing benefits from adding more turbines.

Furthermore, there may exist maximum permissible flow rate reductions, as shown by the contours in figure 3(*c*), due to environmental constraints for which a typical limit is $\hat{Q}/Q_0 = 0.95$ (The Carbon Trust 2011). For the reference case, the maximum return falls just within this assumed environmental constraint; however, careful consideration of the environmental impact is necessary for layout design where the optimal return requires larger attenuation of flow rate. For a quantified understanding, figure 3(*d*) plots the maximum return and channel power coefficients, together with the channel thrust coefficient at which these occur, along contours of the maximum allowable flow reduction. As the constraint is tightened, channel power and thrust fall monotonically (tending to zero as $\hat{Q}/Q_0 \to 1$), but the optimal return is here realised for $\hat{Q}/Q_0 = 0.95$, and movement away from this optimum decreases the return. Therefore, all else being equal, tightening of the constraint (i.e. reducing flow rate impact) requires the turbine layout to be changed, with reductions in both global blockage (fewer turbines) and local blockage (more spaced out) in order to maximise return and power.

At this optimal return point, the local blockage is relatively high, and the optimal induction factor to maximise the channel power coefficient increases when compared to unblocked and blocked flow models at the same global blockage (Garrett & Cummins 2007). Similar to the two-scale and blocked flow models, this leads to a larger peak operating disc thrust coefficient shown in figure 3(*e*), which needs to be further accounted for in the design of the turbine structure. The root-mean-square thrust can be estimated by dividing the peak thrust by $\sqrt{8/3}$, but, depending on the global blockage, it is likely that power capping control strategies will still be required by real turbines to limit the
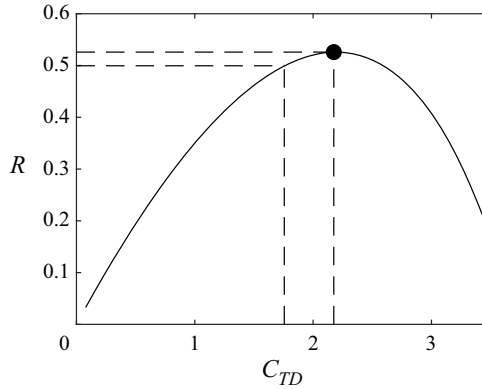
Figure 4. The impact of varying the peak disc thrust coefficient C_{TD} on the return parameter at the optimal design (B_L, B_G) point for the reference flow case shown in figure 3. The impact on return of a 20 % de-rating of the thrust is also shown.

maximum thrust whilst operating at the optimal flow reduction factor as suggested by Vogel, Willden & Houlsby (2019). For instance, figure 4 shows how a controlled reduction in the thrust at the optimal design point for maximising return would impact the return. An example 20 % de-rating from the peak thrust point would decrease the return by only 5 %. Furthermore, such thrust capping may also be necessary only at near peak flow speeds.

Additionally, an increase in extractable power due to non-zero local blockage results in a decrease in the basin efficiency η, the ratio of power extracted by the turbines to the total power removed from the flow (figure 3f) – with the latter necessarily exceeding the former due to the energy lost in wake remixing processes. A minimum allowable basin efficiency could be considered as an additional constraint for optimisation of the return. Here, it is useful to note that a Betz-optimum unblocked wind turbine operates with basin efficiency $2/3$, so for the model parameters set in this reference case, the efficiency of extraction (basin efficiency) does not fall far below the unblocked optimum ($\eta = 0.59$ for maximum return).

Finally, we note that the maximum local blockage is constrained by the depth of the channel. In this case, the optimal return is realised for $(h/d)_{max} \approx 1.5$. For the assumed turbine diameter $d = 20$ m, the channel depth is therefore bounded by $h \leq 30$ m to achieve this optimal blockage ratio in a fence configuration. For deeper channels, alternative non-single-row fence arrangements of turbines are hence necessary to optimise return.

Of further interest is how variations in the channel parameters affect the optimal turbine configuration. In §§3.2 and 3.3, we hence consider variations in the non-dimensional groups governing the channel characteristics, namely the channel Froude number $Fr_\omega = \omega l/\sqrt{ag}$, and the channel friction parameter $C_f(l/h)$.

3.2. *Effect of variation in channel Froude number*

The channel-based Froude number can be interpreted physically as proportional to the square root of the ratio of cycle-averaged driving head to kinetic head (see Appendix A). Therefore, for a fixed driving head, the kinetic head decreases with increasing Froude number, and we might expect a lower return. Figures 5 and 6 illustrate the impact of the channel Froude number on both the fence performance and the environmental impact, respectively. Here, we consider two simple changes to the reference channel flow case.
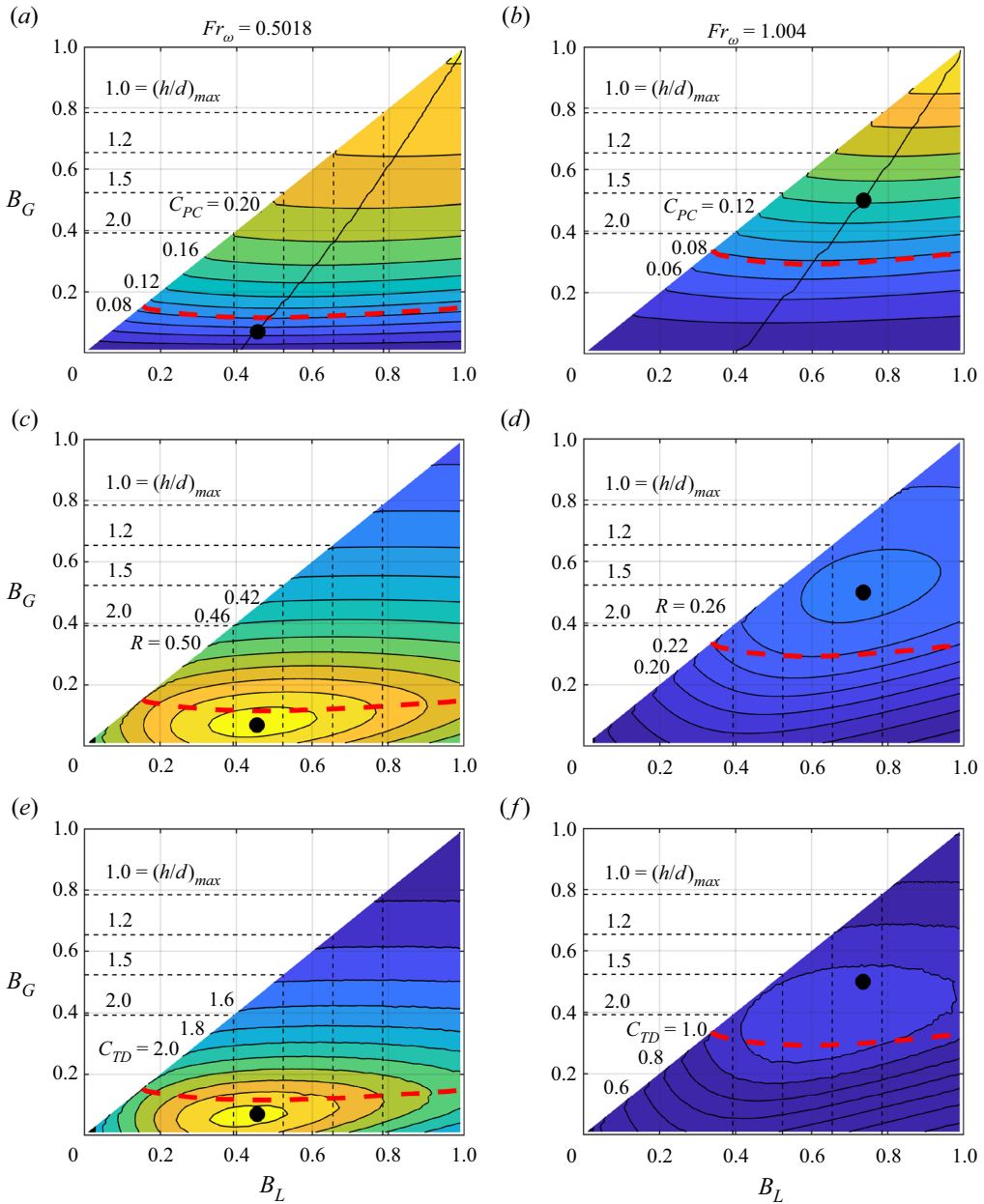
Figure 5. Contours of fence performance comparing (a,c,e) $Fr_\omega = 0.5018$, and (b,d,f) $Fr_\omega = 1.004$, all for $C_f = 0$ and l/h undefined. All presented solutions correspond to the array thrust setting that achieves maximum C_{PC} at the indicated combination of blockage ratios. The black circle represents the maximum return point, and the red dashed line indicates a locus of $\hat{Q}/Q_0 = 0.95$. The dashed lines provide geometric limits on blockages for ratios of channel height h to turbine diameter d. (a,b) The channel power coefficient, with the solid black line indicating the locus of maximum C_{PC} with global blockage; (c,d) the return parameter; (e,f) the disc thrust coefficient.
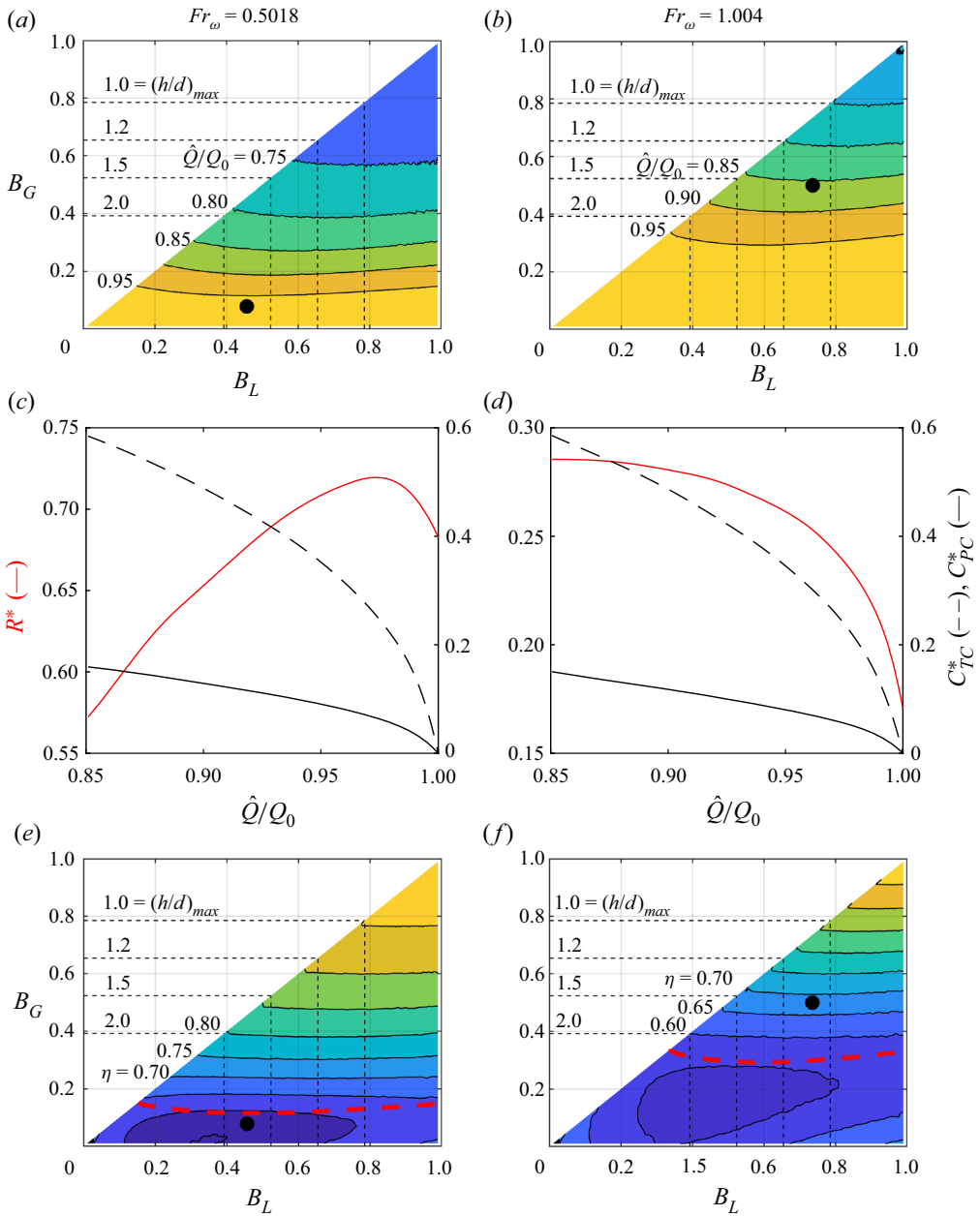
Figure 6. Contours related to channel environmental constraints for (a,c,e) $Fr_\omega = 0.5018$, and (b,d,f) $Fr_\omega = 1.004$, with $C_f = 0$ and l/h undefined. All presented solutions correspond to the array thrust setting that achieves maximum C_{PC} at the indicated combination of blockage ratios. The black circle represents the maximum return point, and the red dashed line indicates the locus of $\hat{Q}/Q_0 = 0.95$. The dashed lines provide geometric limits on ratios of channel height h to turbine diameter d. (a,b) The normalised flow rate; (c,d) the peak return, peak channel power coefficient and corresponding channel thrust coefficient across contours of normalised flow rate; (e,f) the basin efficiency.

In figures 5(*a,c,e*) and 6(*a,c,e*), we assume that the tidal range has risen to $a = 0.8$ m such that $Fr_\omega = 0.5018$ (for the same channel dimensions and tidal frequency), and in figures 5(*b,d,f*) and 6(*b,d,f*) we assume that the tidal range has fallen to $a = 0.2$ m such that $Fr_\omega = 1.004$.

For a fixed global blockage or relative flow rate, there remains an optimal local blockage to maximise the channel power coefficient. However, an increase in channel Froude number for fixed B_G causes the channel power coefficient to decrease (figures 5*a* and 5*b*). For example, in this case for $B_G = 0.2$, C_{PC} falls $\sim 64\%$ through the increase in Fr_ω considered. Interestingly, for either fixed B_G or $\hat{Q}/Q_0$, the optimal spacing B_L for maximising C_{PC} between the two cases does not change. For a fixed number of turbines or fixed environmental constraints, therefore, the channel dynamics impacts only the resultant power output and not the optimal configuration.

By contrast, both the magnitude and location of the maximum return vary significantly with variation in Fr_ω (figures 5*c* and 5*d*). The magnitude of the optimal return increases with decreasing channel Froude number, and is realised at both lower local blockage and global blockage. This is particularly important when considering constraints on the flow reduction, with high Fr_ω channels necessitating a larger move away from the optimum under the same constraint (here plotted for $\hat{Q}/Q_0 = 0.95$). Similar to the reference flow case, as well as the two-scale and blocked flow models, an increase in the return can be correlated broadly to an increase in the disc thrust coefficient (figures 5*e* and 5*f*), with peak C_{TD} of the low Fr_ω case more than three times larger than the high Fr_ω case. Turbines will therefore need to be designed carefully for the specific channel dynamics, and both channel and turbine fence configuration selection are critical for optimal return at a given site.

Figure 6 details the environmental impact of turbines operating in channels of varying Fr_ω. The decreases in C_{PC} with increasing Fr_ω observed in figure 5 correspond to smaller environmental impacts, so the gradients with respect to the global blockage ratio of both the relative flow rate (figures 6*a* and 6*b*) and basin efficiency (figures 6*e* and 6*f*) are likewise smaller. For high Fr_ω channels, the larger B_G and B_L necessary to maximise return and increase channel power C_{PC} are therefore more attainable due to reduced environmental impact. However, for a given flow rate constraint, the maximum return moves further outside of the constraint envelope as Fr_ω increases. This is quantified in figures 6(*c*) and 6(*d*), where for the large Fr_ω case, the maximum return continues to rise with further relaxation of the constraints to $\hat{Q}/Q_0 = 0.85$, whilst for the low Fr_ω case, peak return is achieved at minimal environmental impact ($\hat{Q}/Q_0 \approx 0.98$). Note that although the lower Fr_ω case achieves its maximum return at reduced environmental impact, the power delivered, C_{PC}, is itself lower than in the higher Fr_ω case.

A final consideration for optimising channels with high Fr_ω is that as the optimal blockage ratio increases, the maximum allowable channel depth for a single-row turbine fence configuration falls. For turbines operating in high-Froude-number channels with large depths, interlaced co-planar multi-row arrangements of turbines are a more likely design consideration for optimal energy extraction.

3.3. *Effect of channel bed friction*

We now turn our attention to the effect of $C_f(l/h)$ on both the environmental constraints and array performance. To allow for a clear comparison, the bed-friction coefficient is assumed to be $C_f = 0.002$, and we present the results for the reference case channel Froude number $Fr_\omega = 0.635$. As $C_f(l/h)$ appears combined as a non-dimensional group in (2.1),
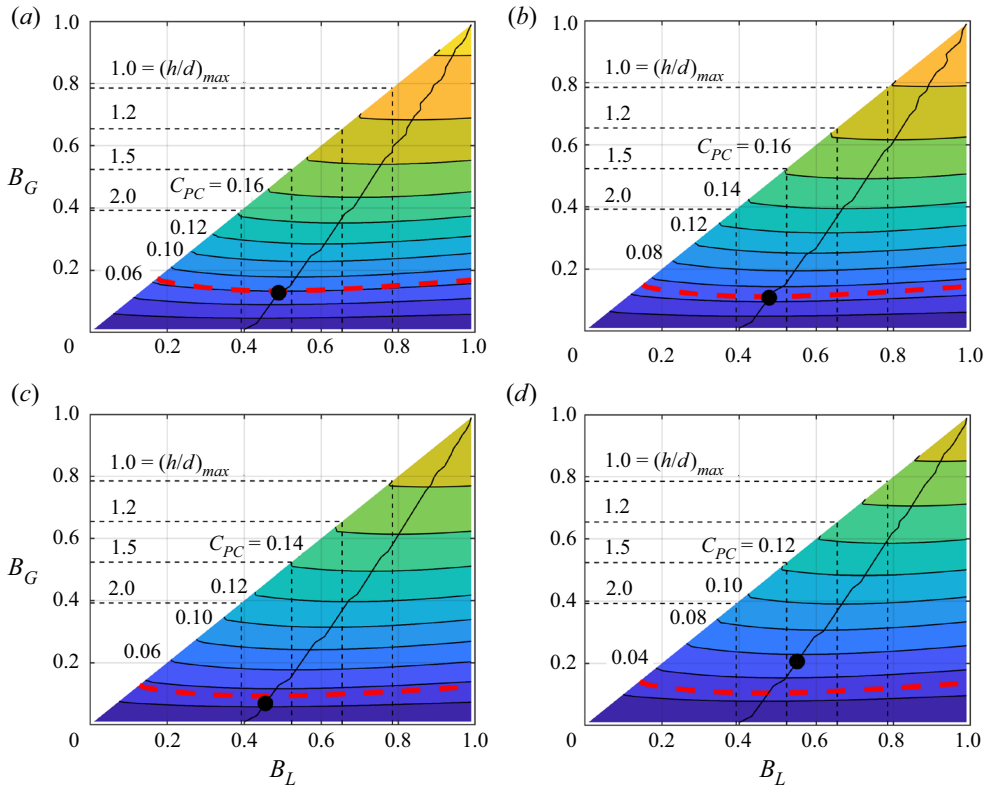
Figure 7. Contours of the channel power coefficient C_{PC} for $Fr_\omega = 0.635$ and $C_f = 0.002$, comparing differences in the impact of bed friction by varying l/h. All presented solutions correspond to the array thrust setting that achieves maximum C_{PC} at the indicated combination of blockage ratios. The black circle represents the maximum return point, and the red dashed line indicates the locus of $\hat{Q}/Q_0 = 0.95$. The dashed lines provide geometric limits on blockages for ratios of channel height h to turbine diameter d: (*a*) $l/h = 50$, (*b*) $l/h = 100$, (*c*) $l/h = 250$ and (*d*) $l/h = 500$.

any change in l/h for a fixed bed friction and fixed channel Froude number is equivalent to holding l/h constant and varying C_f by the same amount. It is also useful to interpret increasing l/h with Fr_ω and C_f fixed as a reduction in channel depth, which should increase the significance of bed friction in the dynamical balance equation. Bed friction and turbine resistance compete with each other to resist the flow, hence for a fixed global blockage (and non-zero bed friction), increases in l/h increase the bed resistance, leading to reductions in the performance of the tidal fence.

Figure 7 illustrates this decrease in channel power with increasing $C_f(l/h)$. For instance, for $B_G = 0.2$, C_{PC} falls by close to 50 % with an increase in l/h from 50 to 500. As with changes in Fr_ω, the C_{PC} locus does not vary with changes in $C_f(l/h)$, suggesting that this locus is universal. A curve fit shows that

$$B_L = \frac{9B_G + 4}{3B_G + 10} \tag{3.2}$$

is a good approximation to estimating the turbine spacing required to maximise power depending on the achievable level of global blockage. We also note that in all cases, the maximum return lies on this locus, but may occasionally lie outside of the acceptable environmental constraint envelope. As $B_G \to 0$, the optimum local spacing is $B_L \to 0.4$,
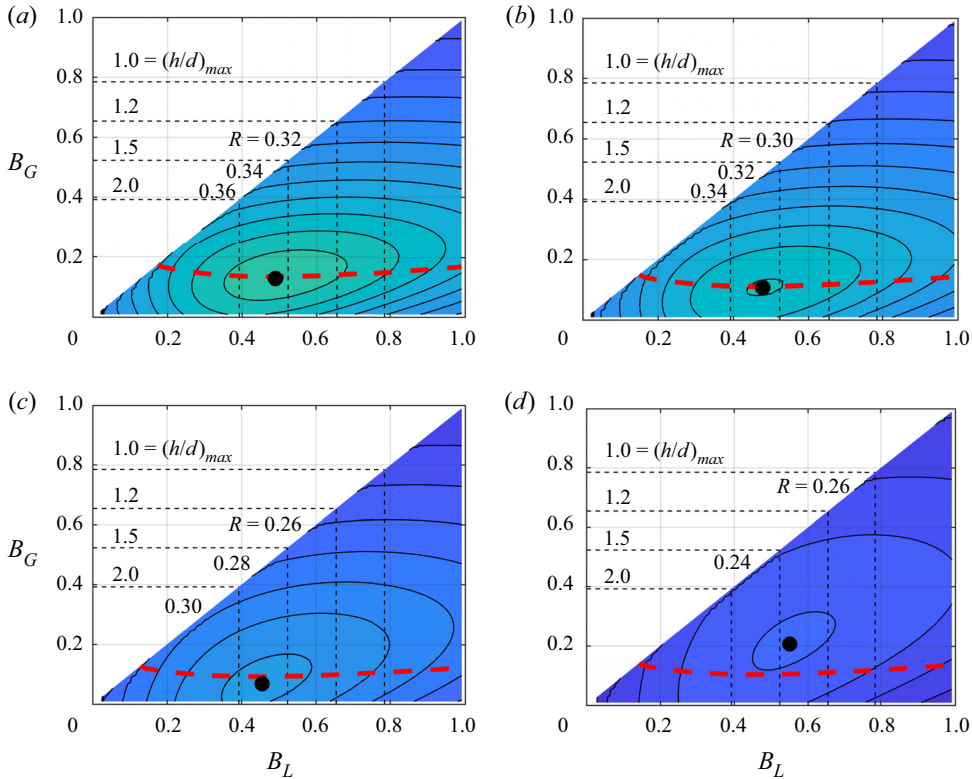
956 A14-16

Figure 8. Contours of the return parameter R for $Fr_\omega = 0.635$ and $C_f = 0.002$, comparing differences in the impact of bed friction by varying l/h. All presented solutions correspond to the array thrust setting that achieves maximum C_{PC} at the indicated combination of blockage ratios. The black circle represents the maximum return point, and the red dashed line indicates the locus of $\hat{Q}/Q_0 = 0.95$. The dashed lines provide geometric limits on blockages for ratios of channel height h to turbine diameter d: (*a*) $l/h = 50$, (*b*) $l/h = 100$, (*c*) $l/h = 250$ and (*d*) $l/h = 500$.

which recovers the local blockage for maximum power found in the partial fence model without channel flow interaction (Nishino & Willden 2012).

The return is shown in figure 8, where we observe that compared to variations in Fr_ω, the blockage ratios required to achieve peak return do not vary nearly as strongly. Although the optimal return decreases monotonically with increasing l/h, the location of the optimal return does not, due to nonlinearity of the governing equation, occurring first at decreasing B_G up to $l/h = 250$ before at increasing B_G for $l/h = 500$. The magnitude of the optimal return is impacted significantly by frictional losses. Additionally, as the integrated bed friction increases, the gradient of the return decreases, and near maximum returns can be realised across a large range of B_L and B_G. Approximately optimal returns can be achieved across a broad range of blockages whose bed friction is significant. By contrast, the low Fr_ω zero bed friction channel (see figure 5*c*) has a steep return gradient, and careful consideration of blockage is necessary to optimise return.

The nominal flow rate Q_0, which for $C_f(l/h) > 0$ is defined to be the channel flow rate without turbines but with bed friction, naturally decreases significantly with increasing bed friction; however, the normalised flow rate $\hat{Q}/Q_0$ shown in figure 9 is not impacted significantly. This stands in contrast to variations in Fr_ω, and implies that an increase in the bed friction does not significantly change the environmental constraints on permissible
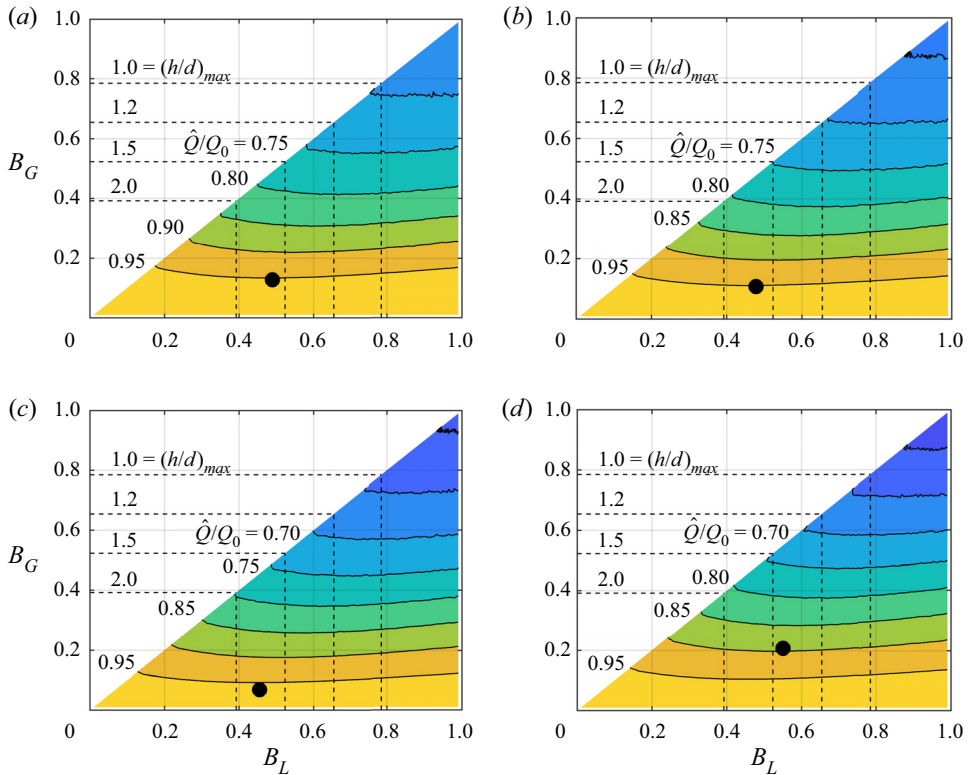
956 A14-17

Figure 9. Contours of the normalised flow rate $\hat{Q}/Q_0$ for $Fr_\omega = 0.635$ and $C_f = 0.002$, comparing differences in the impact of bed friction by varying l/h. All presented solutions correspond to the array thrust setting that achieves maximum C_{PC} at the indicated combination of blockage ratios. The black circle represents the maximum return point. The dashed lines provide geometric limits on blockages for ratios of channel height h to turbine diameter d: (a) $l/h = 50$, (b) $l/h = 100$, (c) $l/h = 250$ and (d) $l/h = 500$.

blockage ratios. For high bed-friction channels, design for large blockage ratios to maximise C_{PC} will be highly constrained by flow rate considerations, principally due to the flow rate reduction caused by the bed friction itself. These observations are consistent with Vennell (2013) and Vennell *et al.* (2015), who observed diminishing returns for additional turbines in channels with high relative bed friction.

3.4. *Designing for maximum return*

Horizontal slices through the return contours at the global blockages for maximum return and for globally unblocked channels are shown in figure 10. For a given set of non-dimensional channel groups, there is always a local blockage B_L that maximises return, and homogeneous spacing that does not exploit the local blockage effect decreases the return in all cases. As the channel Froude number decreases, the optimal global blockage for maximum return falls (figure 10a), and the local blockage effect becomes the primary mechanism for increases in the return. For globally unblocked channels, the local blockage for peak return is identical to the maximum power found in the partial fence model without channel flow interaction (Nishino & Willden 2012), and is lower than optimally blocked channels at the same channel Froude number. The maximum return must, however, be de-rated for increases in the channel bed friction (figure 10b), and for
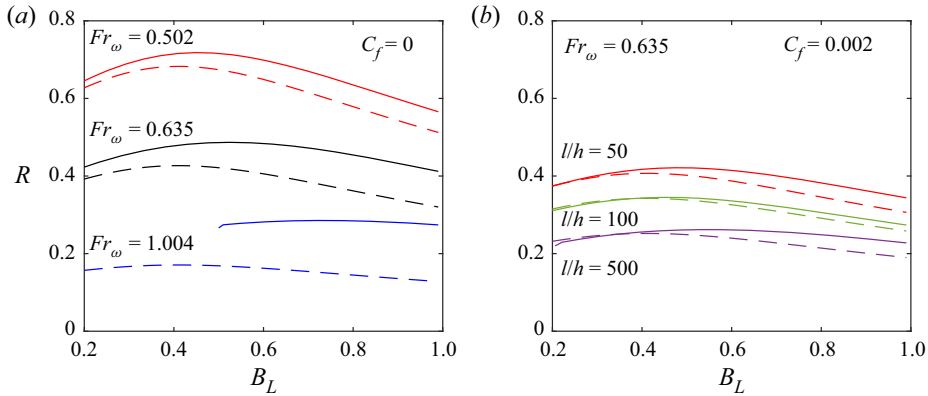
956 A14-18

Figure 10. Slices (at constant B_G) across contour maps of the return at the required global blockage ratio for maximum return (solid lines) and for globally unblocked channels (dashed lines) for which each curve shows a distinct peak with local blockage. (*a*) Plots show how variations in the channel Froude number impact the arrangement for maximising return. The optimal global blockage ratios for peak return are $B_G = 0.07$ for $Fr_\omega = 0.502$, $B_G = 0.17$ for $Fr_\omega = 0.635$ and $B_G = 0.50$ for $Fr_\omega = 1.004$. (*b*) Plots show how variations in the bed friction impact the optimal return arrangement, here for $Fr_\omega = 0.635$ and $C_f = 0.002$. The optimal global blockage ratios for peak return are $B_G = 0.11$ for $l/h = 50$, $B_G = 0.07$ for $l/h = 100$ and $B_G = 0.21$ for $l/h = 500$.

particularly high bed-friction channels, a relatively low maximum return is realised at high global blockage, making such channels difficult to optimise and exploit.

The interplay between these two non-dimensional groups and the maximum return is illustrated in figure 11, where the convergence of the zero global blockage and global blockage for peak return for low Fr_ω is illustrated. The universality of the optimal C_{PC} locus, and the fact that the maximum return must always lie on this curve, imply that figure 11(*b*) and (3.2) can be used to specify the number (B_G) and spacing (B_L) of turbines to optimise return for low bed-friction channels at a given Fr_ω. The required local and global blockages are illustrated in figure 11(*b*) as a function of Fr_ω. This figure gives a simple look-up for B_G^* and B_L^* as a function of Fr_ω for $C_f(l/h) = 0$, which should be very useful for an engineer.

For channels with non-negligible bed friction (in this case for $l/d \geq 50$ with $C_f = 0.002$), the optimal return can be approximated by linearly de-rating the return from the zero friction case (figure 11*c*). The dependency of the return on the optimal blockage is, however, non-monotonic (figure 11*d*), and the turbine layout can be fine-tuned for optimal return by altering B_G. However, recall that the gradients of return with blockage are small for non-zero friction cases, so the optimal returns for globally unblocked and blocked channels lie close together for a wide range of $C_f(l/h)$; hence although an optimum global blockage exists, the return remains rather insensitive to it.

We summarise by including a simple dimensional design example for a new tidal array. Suppose that we wish to install turbines with diameter $d = 20$ m in a tidal channel that is $l = 8$ km long, $h = 30$ m deep and $w = 4$ km wide, with driving head amplitude $a = 0.5$ m. For an initial estimate, assume an idealised channel with no bed friction. First, find the channel-based Froude number $Fr_\omega = \omega l/\sqrt{ga} \approx 0.5$, where we have assumed that the tidal forcing frequency $\omega = 1.4 \times 10^{-4}$ rad s^{-1} is equal to the dominant lunar M_2 frequency. Reading from figure 11(*b*), the optimal blockage ratios are then $B_G^* \approx 0.08$ and $B_L^* \approx 0.46$. The number of turbines for optimal deployment is then $n = whB_G/(\pi d^2/4) \approx 30$. The local blockage $B_L = (\pi d^2/4)/(h(d + s))$ can then be used to calculate the
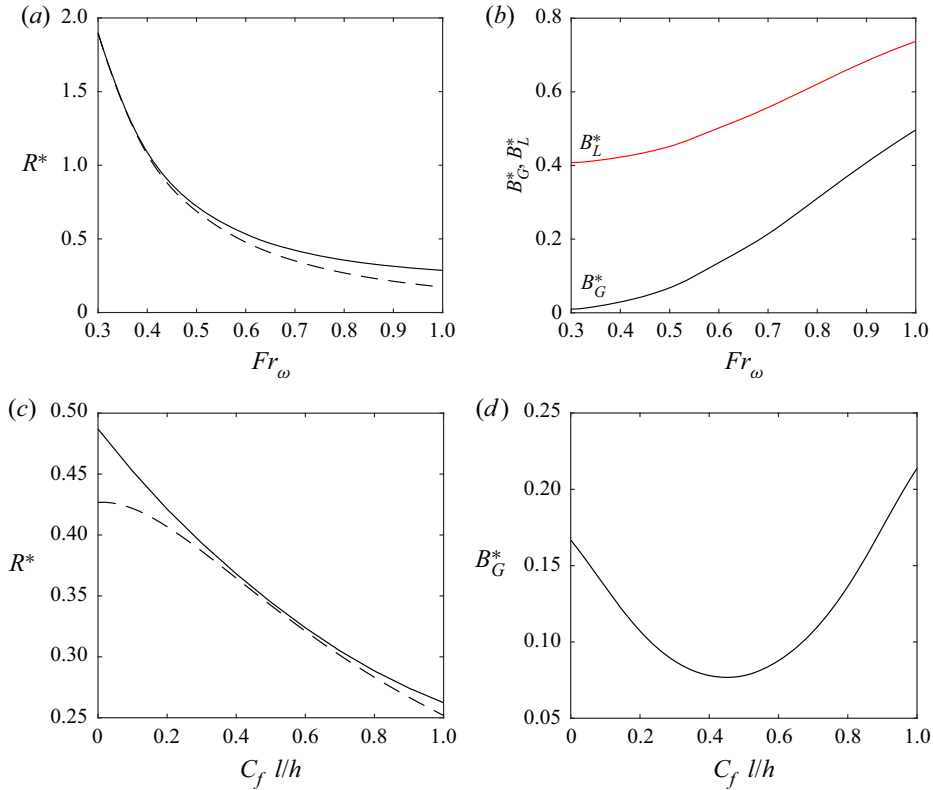
Figure 11. Impact of channel scale non-dimensional groups, the channel Froude number Fr_ω and the channel bed friction $C_f(l/h)$ on the maximum return point. In all plots, the solid line represents the solution for non-zero global blockage; where appropriate, the dashed line represents zero global blockage. For the case of zero bed friction $C_f = 0$, l/h undefined, (*a*) shows the optimal return for non-zero global blockage (solid line) with the corresponding optimal global blockage (black) and local blockage (red) presented in (*b*). Here presented for the $Fr_\omega = 0.635$, $C_f = 0.002$ case, (*c*) shows the optimal return across varying l/h ratios for non-zero global blockage (solid line) with the corresponding optimal global blockage presented in (*d*).

required tip-to-tip spacing s between each turbine such that $s = \pi d^2/(4hB_L) - d \approx 2.8$ m. For this example channel, therefore, a fence of 30 turbines of diameter $d = 20$ m spaced $s = 2.8$ m apart for a total fence width $w_A \sim n(d + s) = 684$ m, representing approximately 17 % the entire width of the channel, is the optimal configuration. The expected return can be read from figure 11(*a*) at $R^* \approx 0.7$, for a channel power coefficient of $C_{PC} = R^* B_G^* = 0.056$. To estimate the power output, first find the peak undisturbed flow rate $Q_0 = (ga/\omega)(wh/l) \approx 526\,000$ m^3 s^{-1}. The optimal time-averaged turbine array power output for the channel is then $n\overline{P_D} = \rho g a Q_0 C_{PC} \approx 144$ MW, with each individual turbine generating $\overline{P_D} = 144/30 = 4.8$ MW. For detailed solutions that take flow rate and thrust constraints into account, as well as layout optimisation for sites with non-negligible bed friction, a solution of the governing equation as outlined in § 2 is recommended.

4. Conclusions

A theoretical model has been proposed to quantify the efficiency of an array of turbines that partially span the width of a tidal channel in which the flow is driven by a sinusoidally

956 A14-20

oscillating head. The framework for this analysis is the two-scale finite fence approach (Nishino & Willden [2012](#)) embedded within and coupled to the one-dimensional channel dynamics model of Garrett & Cummins ([2005](#)). The model hence accounts for both the beneficial constructive interference between turbines in fences that partially span the channel width as well as the coupling between turbine resistance and flow rate, and is an extension of previous models by considering both rough bottom channels and time-dependent oscillatory flow. The model makes no additional assumptions beyond those used in the two models from which it is derived, and the solutions to the non-dimensional equation governing the model are presented. We do note, however, the importance of scale separation assumptions for the combined analytic model. We assume that the device scale mixing takes place much faster relative to the array scale mixing, but that the flow rate through the channel is constant along the length of the channel at any given point in time, and hence that the driving tidal wave is longer than the channel length, which must be considerably larger than the array mixing length scale.

Three non-dimensional groups are shown to fully characterise the flow problem: the channel Froude number group $Fr_\omega = \omega l / \sqrt{ga}$, representing the relative (for a given channel length) oscillatory tidal elevation difference between the two ends of the channel (proportional to the square root of the cycle-averaged potential to kinetic head in the channel); the channel bed-friction group $C_f(l/h)$; and the turbine characteristics group $B_A C_{TA}$. This paper explores the impact of these three groups on both the channel scale flow dynamics and turbine performance characteristics. We introduce the return parameter R, the maximum yield per turbine area, proportional to a ratio of the total power extracted to the total frontal area of the turbines, as an optimisation metric for the arrangement of turbines in a channel. For a given set of channel parameters, which specify the channel Froude number and bed-friction non-dimensional groups, there is an optimal number (B_G) and arrangement (B_L) of turbines to maximise return. By then further considering environmental constraints on the limiting values of acceptable reductions in relative flow rate, basin efficiency and thrust coefficient, we quantify the optimisation envelope for tidal turbine layouts.

We find that blockage plays a major role in the performance of a tidal farm operating in a head-driven flow, with flow reduction in the channel, return parameter and turbine performance strongly influenced by the different scales of blockage. For even relatively unblocked tidal farms, and especially for optimally arranged tidal farms, modelling the channel flow dynamics and resistance is crucial for farm yield estimation. To gain the full benefit of blockage, turbines and their layouts must therefore be carefully designed for their intended blockage environment.

In general, the channel Froude number Fr_ω heavily constrains the maximum possible return, and both channel power and the optimal return decrease as Fr_ω is increased. Increasing Fr_ω, proportional to the square root of cycle-averaged potential to kinetic head, requires high blockage arrangements to extract at optimal power. Increases in the channel bed friction act to decrease the achievable channel power coefficient and to decrease the peak return. Further, increasing bed friction renders sensitivity of flow rate reduction and return optima on local and global blockage ratios less significant. In all cases, the optimal channel power coefficient lies along a universal curve approximated by $B_L = (9B_G + 4)/(3B_G + 10)$, with the maximum return moving along this curve as the channel Froude number and channel bed friction are varied.

Both environmental and engineering constraints heavily restrict the operational envelope of the tidal fence. In general, with increases in Froude number, the channel environmental constraint becomes more restrictive and the device thrust constraint

becomes less restrictive. For thrust coefficients that are larger than achievable by conventional rotors, power capping control strategies are critically important, particularly at peak flow speeds.

This model has great practical potential in aiding tidal turbine developers with detailed knowledge of the channel and frictional characteristics of a candidate site, resulting in a design envelope including both environmental/peak load constraints and the maximum yield point for optimisation in a head-driven tidal channel. The model is also readily applicable to power-limit estimates for resource assessment, and can further be combined with real turbine characteristics to more accurately predict turbine, as opposed to optimal disc, performance.

Author ORCIDs.
- D. Dehtyriov https://orcid.org/0000-0001-6058-9935;
- C.R. Vogel https://orcid.org/0000-0003-2232-9811;
- R.H.J. Willden https://orcid.org/0000-0001-5355-7900.

Appendix A. Non-dimensionalised channel dynamics governing equation

We start with the Garrett & Cummins (2005) model equation, which comes directly from the streamwise integration of the one-dimensional Euler equation

$$c\frac{dQ}{dt} - ag\cos\omega t = -\int_0^l F\,dx, \tag{A1}$$

in which we have assumed smooth inflow and outflow so that the kinetic energy fluxes may be neglected. We assume that the channel cross-section is constant such that $c = \int_0^l A^{-1}\,dx = l/A_C$.

Here, F is the total resistive force per unit mass, which may be distributed arbitrarily along the channel length. The force of the turbines is given by

$$F_T = \tfrac{1}{2}\rho U_C^2 A_C C_{TC} = \tfrac{1}{2}\rho U_C^2 A_C C_{TA} B_A, \tag{A2}$$

and the bed shear stress is given by

$$\tau_b = \tfrac{1}{2}\rho U_C^2 C_f, \tag{A3}$$

which, integrated over the bed surface, gives the resistive force due to bed friction:

$$F_b = \tau_b A_b = \tau_b A_C \frac{l}{h} = \frac{1}{2}\rho U_C^2 A_C \frac{l}{h} C_f. \tag{A4}$$

The total force per unit mass F (where $\rho A_C l$ is the mass of fluid in the channel) is therefore

$$F = \frac{1}{\rho A_C l}\left(\frac{1}{2}\rho U_C^2 A_C C_{TA} B_A + \frac{1}{2}\rho U_C^2 A_C \frac{l}{h} C_f\right), \tag{A5}$$

and substituting this into (A1) gives

$$\frac{\mathrm{d}Q}{\mathrm{d}t} = \frac{ag}{c}\cos\omega t - \frac{1}{\rho A_C c}\left(\frac{1}{2}\rho U_C^2 A_C C_{TA}B_A + \frac{1}{2}\rho U_C^2 A_C \frac{l}{h}C_f\right), \tag{A6}$$

which results in the channel equation including arbitrary resistance from turbines and bed shear.

By non-dimensionalising with $t' = t\omega$, $Q' = Q/Q_0$, where $Q_0 = ga/(\omega)(wh/l) = ga/\omega c$, this simplifies to

$$\frac{\mathrm{d}Q'}{\mathrm{d}t'} = \cos(t') - \frac{U_C^2}{2ga}\left(C_{TA}B_A + C_f\frac{l}{h}\right), \tag{A7}$$

and as by definition $Q = U_C A_C$ so $U_C = Q/A_C = Q'(ga/\omega c A_C)$, we can write

$$\frac{\mathrm{d}Q'}{\mathrm{d}t'} = \cos(t') - Q'^2\frac{ga}{2\omega^2 l^2}\left(C_{TA}B_A + C_f\frac{l}{h}\right). \tag{A8}$$

Defining a non-dimensional channel Froude number as $Fr_\omega = \omega l/\sqrt{ga}$, this can be rewritten as the non-dimensional model equation

$$\frac{\mathrm{d}Q'}{\mathrm{d}t'} = \cos(t') - \frac{1}{2}Q'^2\frac{1}{Fr_\omega^2}\left(C_{TA}B_A + C_f\frac{l}{h}\right), \tag{A9}$$

which is the form of the non-dimensional equation first presented in Willden *et al.* (2014), solved for in this paper.

Equation (A1) carries units of energy per unit mass, so the cycle-averaged energy supplied to the channel by the driving head is given by

$$\bar{E}_\zeta = \frac{1}{T}\int_0^T |ag\cos\omega t|\,\rho A_C l\,\mathrm{d}t = \frac{2\rho l^2\omega}{\pi}Q_0, \tag{A10}$$

where $T = 2\pi/\omega$ is the cycle period. Similarly, in the absence of flow resistance so that $Q = Q_0\sin\omega t = A_C U_C$, the cycle-averaged channel kinetic energy is given by

$$\bar{E}_k = \frac{1}{T}\int_0^T \frac{1}{2}\rho A_C l U_C^2\,\mathrm{d}t = \frac{\rho l}{4A_C}Q_0^2, \tag{A11}$$

so the channel-based Froude number

$$Fr_\omega = \sqrt{\frac{\pi}{8}}\left(\frac{\bar{E}_\zeta}{\bar{E}_k}\right)^{1/2} \tag{A12}$$

may be interpreted usefully as being proportional to the square root of the ratio of the cycle-averaged driving head to kinetic head in the channel.

REFERENCES

ADCOCK, T.A.A., DRAPER, S., HOULSBY, G.T., BORTHWICK, A.G.L. & SERHADLIOĞLU, S. 2013 The available power from tidal stream turbines in the Pentland Firth. *Proc. R. Soc. Lond.* A*: Math. Phys. Engng Sci.* **469** (2157), 20130072.
BLANCHFIELD, J., GARRETT, C., WILD, P. & ROWE, A. 2008 The extractable power from a channel linking a bay to the open ocean. *Proc. Inst. Mech. Engrs* A*: J. Power Energy* **222** (3), 289–297.

BONAR, P.A.J., CHEN, L., SCHNABL, A.M., VENUGOPAL, V., BORTHWICK, A.G.L. & ADCOCK, T.A.A. 2019 On the arrangement of tidal turbines in rough and oscillatory channel flow. *J. Fluid Mech.* **865**, 790–810.

BRYDEN, I.G. & COUCH, S.J. 2007 How much energy can be extracted from moving water with a free surface: a question of importance in the field of tidal current energy? *Renew. Energy* **32** (11), 1961–1966.

COOKE, S.C, WILLDEN, R.H.J., BYRNE, B., STALLARD, T. & OLCZAK, A. 2015 Experimental investigation of tidal turbine partial array theory using porous discs. In *Proceedings of the 11th European Wave and Tidal Energy Conference, Nantes, France*.

CREED, M.J., DRAPER, S., NISHINO, T. & BORTHWICK, A.G.L. 2017 Flow through a very porous obstacle in a shallow channel. *Proc. R. Soc. Lond.* A*: Math. Phys. Engng Sci.* **473** (2200), 20160672.

CUMMINS, P.F. 2013 The extractable power from a split tidal channel: an equivalent circuit analysis. *Renew. Energy* **50**, 395–401.

DEHTYRIOV, D., SCHNABL, A.M., VOGEL, C.R., DRAPER, S., ADCOCK, T.A.A. & WILLDEN, R.H.J. 2021 Fractal-like actuator disc theory for optimal energy extraction. *J. Fluid Mech.* **927**, A40.

DRAPER, S. & NISHINO, T. 2014 Centred and staggered arrangements of tidal turbines. *J. Fluid Mech.* **739**, 72–93.

GARRETT, C. & CUMMINS, P. 2005 The power potential of tidal currents in channels. *Proc. R. Soc. Lond.* A*: Math. Phys. Engng Sci.* **461** (2060), 2563–2572.

GARRETT, C. & CUMMINS, P. 2007 The efficiency of a turbine in a tidal channel. *J. Fluid Mech.* **588**, 243–251.

GUPTA, V. & YOUNG, A.M. 2017 A one-dimensional model for tidal array design based on three-scale dynamics. *J. Fluid Mech.* **825**, 651–676.

KARSTEN, R.H., MCMILLAN, J.M., LICKLEY, M.J. & HAYNES, R.D. 2008 Assessment of tidal current energy in the Minas Passage, Bay of Fundy. *Proc. Inst. Mech. Engrs* A*: J. Power Energy* **222** (5), 493–507.

MCNAUGHTON, J., CAO, B., NAMBIAR, A., DAVEY, T., VOGEL, C.R. & WILLDEN, R.H.J. 2022 Constructive interference effects for tidal turbine arrays. *J. Fluid Mech.* **943**, A38.

MUCHALA, S. & WILLDEN, R.H.J. 2017 Impact of tidal turbine support structures on realizable turbine farm power. *Renew. Energy* **114**, 588–599.

NISHINO, T. & WILLDEN, R.H.J. 2012 The efficiency of an array of tidal turbines partially blocking a wide channel. *J. Fluid Mech.* **708**, 596–606.

NISHINO, T. & WILLDEN, R.H.J. 2013 Two-scale dynamics of flow past a partial cross-stream array of tidal turbines. *J. Fluid Mech.* **730**, 220–244.

O'HARA, M.R. & GALLEGO, A. 2017 A modelling study of the tidal stream resource of the Pentland Firth, Scotland. *Renew. Energy* **102**, 326–340.

SUTHERLAND, G., FOREMAN, M. & GARRETT, C. 2007 Tidal current energy assessment for Johnstone Strait, Vancouver Island. *Proc. Inst. Mech. Engrs* A*: J. Power Energy* **221** (2), 147–157.

THE CARBON TRUST 2011 Carbon trust foreword to UK tidal current resource and economics study. *Tech. Rep.* Black & Veatch Ltd.

VENNELL, R. 2010 Tuning turbines in a tidal channel. *J. Fluid Mech.* **663**, 253–267.

VENNELL, R. 2013 Exceeding the Betz limit with tidal turbines. *Renew. Energy* **55**, 277–285.

VENNELL, R. & ADCOCK, T.A.A. 2014 Energy storage inherent in large tidal turbine farms. *Proc. R. Soc. Lond.* A*: Math. Phys. Engng Sci.* **470** (2166), 20130580.

VENNELL, R., FUNKE, S.W., DRAPER, S., STEVENS, C. & DIVETT, T. 2015 Designing large arrays of tidal turbines: a synthesis and review. *Renew. Sustain. Energy Rev.* **41**, 454–472.

VOGEL, C.R., HOULSBY, G.T. & WILLDEN, R.H.J. 2016 Effect of free surface deformation on the extractable power of a finite width turbine array. *Renew. Energy* **88**, 317–324.

VOGEL, C.R., WILLDEN, R.H.J. & HOULSBY, G.T. 2019 Tidal stream turbine power capping in a head-driven tidal channel. *Renew. Energy* **136**, 491–499.

WHELAN, J.I., GRAHAM, J.M.R. & PEIRÓ, J. 2009 A free-surface and blockage correction for tidal turbines. *J. Fluid Mech.* **624**, 281–291.

WILLDEN, R.H.J., NISHINO, T. & SCHLUNTZ, J. 2014 Tidal stream energy: designing for blockage. In *Proceedings of the 3rd Oxford Tidal Energy Workshop, Oxford, UK*. Tidal Energy Research Group, University of Oxford.